Article:
Terry-Jack, Mohammed and O'Keefe, Simon (2023) Classifying 1D elementary cellular automata with the 0-1 test for chaos. Physica D: Nonlinear Phenomena. 133786. ISSN: 0167-2789

https://doi.org/10.1016/j.physd.2023.133786

Physica D 453 (2023) 133786

Contents lists available at ScienceDirect

Physica D

journal homepage: www.elsevier.com/locate/physd

Classifying 1D elementary cellular automata with the 0–1 test for chaos

Mohammed Terry-Jack *, Simon O'Keefe

University of York, Heslington, York, YO10 5DD, UK

ARTICLE INFO

Article history:
Received 25 March 2023
Received in revised form 29 April 2023
Accepted 10 May 2023
Available online 16 May 2023

Keywords:
0–1 test for chaos
Cellular automata
Wolfram
Chaos
Complexity
Chua complexity index

ABSTRACT

We utilise the 0–1 test to automatically classify *elementary cellular automata*. The quantitative results of the 0–1 test reveal a number of advantages over Wolfram's qualitative classification. For instance, while almost all rules classified as chaotic by Wolfram were confirmed as such by the 0–1 test, there were two rules which were revealed to be non-chaotic. However, their periodic nature is hidden by the high complexity of their spacetime patterns and not easy to see without looking very carefully. Comparing each rule's chaoticity (as quantified by the 0–1 test) against its intrinsic complexity (as quantified by its Chua complexity index) also reveals a number of counter-intuitive discoveries; i.e. non-chaotic dynamics are not only found in simpler rules, but also in rules as complex as chaos.

1. Introduction

Cellular Automata (CAs) are able to exhibit dynamics which are astonishingly complicated [1] and even unpredictable [2], despite their trivially simple composition. Chaos is one of the most interesting and appealing kind of dynamic which CAs exhibit [3], and of direct relevance to a number of fields, ranging from random number generators and cryptography [4] to cardiac arrhythmias [5] and the stability of celestial orbits.

Wolfram [6] proposed the existence of four classes of CA behaviour (of which one is chaos). Unfortunately, without precisely formalised mathematical definitions for each class, there is no effective criteria for membership, nor any quick tests to distinguish classes from one another [2,3,7–10]. Therefore, many successive works in the field have tried to find well-formalised classifications, utilising various ways to quantify interesting characteristics [11]. However, a universally accepted mathematical definition of chaos still does not exist [1,2,8,10,12–16].

Lyapunov exponents have been widely used to determine whether a dynamical system is chaotic or not [5,17,18], but it is important to realise that a positive Lyapunov exponent is not a direct indication of chaos [19] but of *sensitive dependence on initial conditions*, which is a necessary but insufficient condition of chaos [17]. More recently, the *0–1 test for chaos* has been proposed as a simple binary test for distinguishing between regular and chaotic dynamics [5,18,20,21]. Unlike computing the maximal Lyapunov exponent, this test is straightforward to implement [20,22] and computationally inexpensive [18,21,22]. It is even able to detect weak chaos [22] and transitions that occur without Lyapunov exponents turning positive [21]. We have, therefore, implemented the 0–1 Test in python (available at our github page[1]) and are the first to utilise it to classify *Elementary Cellular Automata* (ECA).

This paper is organised as follows: Section 2 introduces various definitions related to ECAs and their local dynamics, Section 3 expands on the global dynamics of interest, i.e. Chaos (3), and Section 4 introduces definitions related to the 0–1 Test for Chaos. Section 5 specifies the pseudocode for the 0–1 test (algorithm 1), the exact test settings and ECA parameters used (5.1) and the resulting classification (Table 3). Section 5.2 analyses the types of spectral patterns observed (5.2.1), compares the results against Wolfram's famous classification (5.2.2) and investigates the relationship between each rule's *chaoticity* and *complexity* (5.2.3). Section 6 discusses the importance of the *initial configuration* (IC) on CA dynamics (6.1), some advantages and disadvantages of the 0–1 test (6.2) and the difference between chaos and *randomness* (6.3).

2. Cellular automata

Cellular Automata (CA) have received growing attention as formal models for complex systems with applications in almost every scientific domain [3,16].

* Corresponding author.
E-mail addresses: mdtj500@york.ac.uk (M. Terry-Jack), simon.okeefe@york.ac.uk (S. O'Keefe).

[1] https://github.com/mohammedterryjack/0-1Test

https://doi.org/10.1016/j.physd.2023.133786

2.1. 1D-ECAs

Below we introduce the simplest kind of CA that exists, defining its composition and key dynamical properties it can exhibit over time.

Definition 1. An *Elementary Cellular Automaton* ***(ECA)*** is a one-dimensional, dynamical system in which space and time are discrete. Let $r \in \mathbb{N} : r \geq 1$ be the *neighbourhood radius*. Space is represented by a regular lattice of $W \in \mathbb{N} : W \geq 2r+1$ identical, locally-interconnected *cells* (finite automata) with a binary state space, $\mathbb{S} = \{0, 1\}$.

Definition 2. The ECA's ***global state***, $x \in \mathbb{S}^W$, is a lattice configuration specified by the values of all the states of all cells in the lattice at a given time.

Definition 3. A lattice x is ***spatially periodic*** iff $\exists\, s \in \mathbb{N} : s \geq 1$ s.t. $\forall w \in [0, W-s)$:

$$x_w = x_{w+s} \tag{1}$$

where the least s with such a property is the *spatial period*. When $s = 1$, x is *homogeneous*.

Definition 4. This state evolves deterministically in synchronous, discrete time steps according to a ***global map*** $g_\rho : \mathbb{S}^W \to \mathbb{S}^W$ defined by a *local rule* $\rho : \mathbb{S}^{2r+1} \to \mathbb{S}$ (Section 2.2) which acts on the value of each single cell on the basis of the cell's present state and those of a finite set of neighbouring cells

$$[g_\rho(x)]_w = \rho(x_{w-r}, \ldots, x_w, \ldots, x_{w+r}) \tag{2}$$

Definition 5. The sequence of states an ECA passes through during its *space–time evolution*, $\mathcal{O}^T(x) =$ $[x, g_\rho(x), g_\rho(g_\rho(x)), \ldots, g_\rho^{\circ T-1}(x)]$, defines its ***trajectory*** (also referred to as its *orbit*) from an *initial condition* (configuration) x for $T \in \mathbb{N} : T \geq 1$ finite time steps to be observed, and can be compactly written as:

$$[\mathcal{O}^T(x)]_t = g_\rho^{\circ t}(x) \tag{3}$$

Definition 6 (*or simply* periodic)**.** A trajectory $\mathcal{O}(x)$ is ***temporally periodic*** iff $\exists\, \tau \in \mathbb{N} : \tau \geq 1$ s.t. $\forall t \in [0, T-\tau)$:

$$[\mathcal{O}^T(x)]_t = [\mathcal{O}^T(x)]_{t+\tau} \tag{4}$$

where the least τ with such a property is called the *temporal period*. When $\tau = 1$, x is a *fixed point*.

Definition 7. Let $dist|x, y|$ denote the distance between any two points $x, y \in \mathbb{S}^W$, s.t. $dist|x, x| = 0$ and $dist|y, y| = 0$. A trajectory $\mathcal{O}^T(x)$ is ***regular*** if it has a dense orbit (i.e. it remains arbitrarily close to the orbits of all sufficiently close configurations) $\exists \varepsilon \in \mathbb{R}$: $\varepsilon > 0$ s.t. $\forall t \in [0, T-\tau)$:

$$dist|[\mathcal{O}^T(x)]_t\ ,\ [\mathcal{O}^T(x)]_{t+\tau}| \leq \varepsilon \tag{5}$$

$[\mathcal{O}^T(x)]_t$ is an *equicontinuity point* if $\mathcal{O}^T(x)$ is regular (*equicontinuous*) with period τ.

Definition 8. $\mathcal{O}^T(x)$ is ***almost equicontinuous*** if for some $\varepsilon \in \mathbb{R} : \varepsilon > 0$ there exists at least one $t \in [0, T-\tau)$:

$$dist|[\mathcal{O}^T(x)]_t\ ,\ [\mathcal{O}^T(x)]_{t+\tau}| \leq \varepsilon \tag{6}$$

Definition 9. Sensitive dependence on initial conditions describe trajectories wherein infinitesimally small differences in their initial condition grow exponentially, on-average, into macroscopic-scale divergences [15,23–25]. Thus we can say $\mathcal{O}^T(x)$ is *sensitive* if the trajectories of at least two nearby points eventually separate by some *sensitivity constant* $\delta \in \mathbb{N} : \delta > \varepsilon$. Let $N(x) = \{n \in \mathbb{S}^W \mid 0 < dist|n, x| \leq \varepsilon\}$ denote points arbitrarily close to x. A trajectory $\mathcal{O}^T(x)$ is *sensitive* iff $\exists\, t \in \mathbb{N} : t \geq 1$:

$$\exists y \in N(x) : \quad dist|[\mathcal{O}^T(x)]_t\ ,\ [\mathcal{O}^T(y)]_t| \geq \delta \tag{7}$$

Definition 10 (*a stricter form of sensitive dependence*)**.** A trajectory $\mathcal{O}^T(x)$ is *positively* ***expansive*** if *all* points arbitrarily close to x diverge over time:

$$\forall y \in N(x) : \quad dist|[\mathcal{O}^T(x)]_t\ ,\ [\mathcal{O}^T(y)]_t| \geq \delta \tag{8}$$

It is thus straightforward to verify that positively expansive ECAs are also sensitive

Definition 11 (*or topological* mixing)**.**Topological transitivity describes how well a transformation mixes up its domain. The highest and lowest forms of mixing are called *Bernoulli* and *Ergodic*, respectively [19]. A trajectory $\mathcal{O}^T(x)$ is topologically ***transitive*** iff $\exists\, t \in \mathbb{N} : t \geq 1$ s.t. for any pair of non-empty sets $X, Y \subset \mathbb{S}^W$

$$X \cap [\mathcal{O}^T(Y)]_t \neq \emptyset \tag{9}$$

where $[\mathcal{O}^T(Y)]_t = \{[\mathcal{O}^T(y)]_t \mid y \in Y\}$ denotes all possible future states resulting from the trajectories of each state y in the set Y after t time steps.

2.2. Local rule ρ

Below we expand upon the concept of the local rule which lies at the heart of every CA (according to Definition 4). For the simplest case of 1D ECA (i.e. with nearest-neighbourhood coupling, $r = 1$) there are 256 possible local rules.

2.2.1. Tabular form

Conventionally, a local rule ρ is expressed as a truth table (e.g. Table 1) and referred to by the value of its output sequence, in decimal (e.g. $0001110_2 = 14_{10}$).

Table 1
Lookup table for Rule 14 (ρ_{14})

v_1	v_2	v_3	$\rho_{14}(v)$
0	0	0	0
0	0	1	1
0	1	0	1
0	1	1	1
1	0	0	1
1	0	1	0
1	1	0	0
1	1	1	0

2.2.2. Hypercube representation

A rich range of mathematical characteristics can be found in the local rules, many of which become more apparent when reformulated into functional form. For example, the boolean hypercube representation [26,27] is a geometrical approach which allows for ECA rules to be easily expressed in unique yet generic boolean equations (each representing a limited number of geometric configurations on the hypercube). Every input $v \in \mathbb{S}^{2r+1}$ of the local rule's truth table gets mapped onto exactly one of the n coloured vertices in a $(2r+1)$-dimensional unit hypercube (where the colour represents the corresponding output, $\rho(v_1, \ldots, v_{2r}, v_{2r+1}) \in \mathbb{S}$). The set of true points, $V_\top \subseteq \mathbb{S}^{2r+1}$, and the set of false points, $V_\bot \subseteq \mathbb{S}^{2r+1}$, correspond to the specific inputs yielding a 1 or 0, respectively (i.e. the edges of the hypercube which are coloured or not). For ECA rules, the true and false points do not intersect, $V_\top \cap V_\bot = \emptyset$. E.g. an ECA with

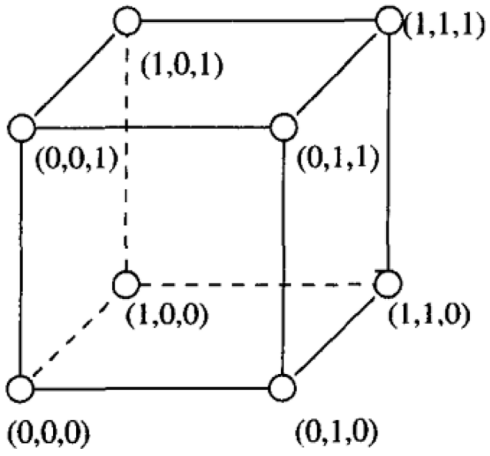

Fig. 1. 3D hypercube representation.

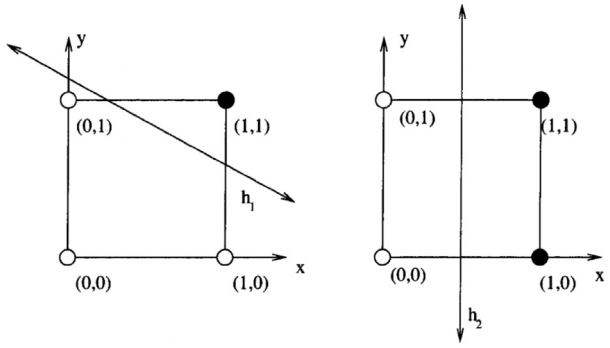

Fig. 2. A couple of example threshold functions represented as 2D hypercubes. A single 1D hyperplane $h \in \mathbb{R}^2$ is able to separate their true and false points, demonstrating their linear separability.

neighbourhood radius $r = 1$ would thus have 8 unique inputs in its truth table, corresponding to the $n = 8$ vertices on a $(2r+1 =)$ 3-dimensional hypercube (Fig. 1). For 3-dimensional hypercubes, there are exactly 14 unique configurations (with corresponding boolean or algebraic expressions) that compactly represent all ECA rules (Table 5).

2.2.3. Threshold functions

Linearly separable hypercubes are geometrical representations of *threshold* functions (or *regular* functions [27]) — i.e. functions producing a set of true points, $V_\top$, that can be separated from the set of false points, $V_\perp$, by a single hyperplane (known as the *separator* or separating *structure*)(see Figs. 2 and 3).

Definition 12. A local rule, ρ, is a ***threshold function*** iff $\exists\ h \in \mathbb{R}^{2r+1}$ s.t.

$$min\{h \cdot v_\top \mid v_\top \in V_\top\} > max\{h \cdot v_\perp \mid v_\perp \in V_\perp\} \tag{10}$$

3. Deterministic chaos

Despite being composed of trivially simple elements, ECAs exhibit a variety of dynamical behaviours, some of which are astonishingly complicated [1] and even unpredictable [2], including self-organisation, fractals, chaos and many complex features [15] (most of which are not completely understood yet [3]).

Chaos is one of the most interesting and appealing kinds of dynamical behaviours that can be found among CAs [3]. Being able to distinguish between regular and chaotic dynamics is an important question with applications ranging from random number generators and cryptography [4] to cardiac arrhythmias [5] and the stability of celestial orbits.

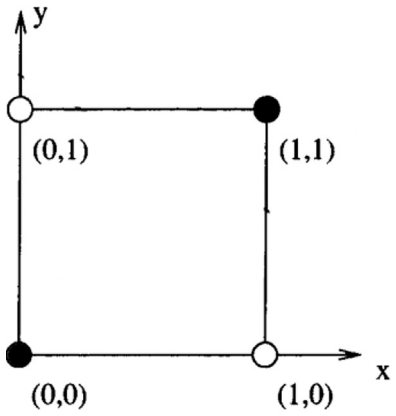

Fig. 3. This 2d hypercube represents the function $\rho(a, b) = ab \vee \overline{ab}$, which is not a threshold function because its set of true points are $V_\top = \{(0, 0), (1, 1)\}$ and its set of false points are $V_\perp = \{(0, 1), (1, 0)\}$ and they are not linearly separable.

Chaos is a phenomenon governed entirely by an underlying, deterministic process [12,16,28] (i.e. its future is completely determined by the past, such that $[\mathcal{O}^T(x)]_{t+1}$ is related to $[\mathcal{O}^T(x)]_t$ by some functional relation g_ρ). As such, chaotic systems are quite predictable in the short term [12,17] and may even allow for accurate forecasts beyond the near future, well into the medium range [19,24]. However, it becomes impossible to predict in the long run [12,19,23,24], which seems paradoxical; unpredictable determinism [12,29]!

Chaos creates unpredictability where none existed before via *sensitive dependence on initial conditions* [12] (Definition 9), which means initial sensitivities (i.e. small uncertainties or errors in the input introduced by round-off imprecision inherent in all instruments) get amplified (as the predicted trajectory diverges from the true orbit) and lead to catastrophic errors in the final output.

3.1. Defining chaos

So what are the signs of chaos? How can they be measured? What precisely are the properties of strange chaotic attractors that can be quantified? Unfortunately, a universally accepted mathematical definition of chaos does not yet exist [1,2,8,10,12–16]. Capturing chaos in a single definition is difficult since its manifestations can be varied and a general, unified theory for this scientific phenomenon (which is still far from being completely understood) is lacking [3,17,19].

Nevertheless, several different mathematically precise attempts to quantify chaos have been proposed, each based on different backgrounds and levels of mathematical sophistication [1,14,24,29,29].

Definition 13. Devaney's definition marked the point where chaos (as a mathematical notion) became popular and began to enter university textbooks [1,29]. A trajectory $\mathcal{O}^T(x)$ is ***D-chaotic*** (chaotic inspired by Devaney's definition of chaos) iff:

D1: $\mathcal{O}^T(x)$ is *transitive* (Definition 11)
D2: $\mathcal{O}^T(x)$ is *regular* (Definition 7)
D3: $\mathcal{O}^T(x)$ is *sensitive* (Definition 9)

D-chaos is a purely topological definition and, as such, one of the simpler definitions. It was actually found to contain redundancies (D1 and D2 imply D3 in any metric system [2,8,12,29,30]) and can therefore be made even simpler (which is ironic since sensitivity, the hallmark of chaos, turns out to be superfluous in its definition [29]).

Unfortunately, the shift map (a very simple ECA which just shifts the content of configurations one step to the left) would be considered chaotic according to Devaney's definition. However, the lack of aperiodic motion in a shift map makes it the kind of system people would not intuitively consider chaotic. In fact, this counter-intuitive result seems to be more an artefact of Devaney's definition (and Cantor topology) than any intrinsic chaoticity present in the shift map itself [3].

Definition 14. Knudsen's definition of chaos attempts to remedy this by excluding dynamics without aperiodic motion [31]. A trajectory $\mathcal{O}^T(x)$ is ***K-chaotic*** (chaotic according to Knudsen's definition of chaos) iff:

K1: $\mathcal{O}^T(x)$ is *regular* (Definition 7)
K2: $\mathcal{O}^T(x)$ is *sensitive* (Definition 9)

Definition 15. Expansive chaos is similar to Devaney's definition of chaos, except sensitivity is replaced with positive expansivity (a stronger form of sensitivity) [25,32]. A trajectory $\mathcal{O}^T(x)$ is ***E-chaotic*** (positively expansive chaotic) iff:

E1: $\mathcal{O}^T(x)$ is *transitive* (Definition 11)
E2: $\mathcal{O}^T(x)$ is *regular* (Definition 7)
E3: $\mathcal{O}^T(x)$ is *positively expansive* (Definition 10)

3.2. Testing for chaos

3.2.1. Lyapunov exponents

Many definitions of chaos are based on the notion of sensitivity in some way and it is widely recognised as a central notion in chaos theory [2,12,12,15]. Many even assume it to be the single most significant attribute of chaotic attractors [33] and a property which all chaotic systems definitely have [12].

Lyapunov exponents can be used to detect *sensitive dependence on initial conditions* [24] and are, therefore, are popular indicator of a system's chaoticity [12] and one of the first tests developed for determining whether a dynamical system is chaotic or not [5,17,18] (a bounded deterministic system is considered chaotic if it has at least one positive Lyapunov exponent [12,16–19,24]).

A Lyapunov exponent, λ, quantifies the instantaneous rate of change of infinitesimally small perturbations in state space [16,24,33]. By comparing a trajectory $\mathcal{O}^T(x)$ belonging to some initial condition x with a trajectory $\mathcal{O}^T(y)$ for an initial condition which carries an error $y \in N(x) : dist|x, y| \neq 0$, we can quantify how the error amplifies during the course of the iteration. Specifically, the Lyapunov exponent, λ, characterises the average logarithmic growth of the relative error per iteration [12]:

$$\lambda = \lim_{t\to\infty} \frac{1}{T} \sum_{t=0}^{T-1} \ln \frac{dist|\ [\mathcal{O}^T(x)]_{t+1}\ ,\ [\mathcal{O}^T(y)]_{t+1}\ |}{dist|\ [\mathcal{O}^T(x)]_t\ ,\ [\mathcal{O}^T(y)]_t\ |} \tag{11}$$

A negative Lyapunov exponent $\lambda \leq 0$ means nearby trajectories remain close to each other [17,18] while a positive Lyapunov exponent $\lambda > 0$ indicates an exponential divergence of nearby trajectories (i.e. a small error will be scaled exponentially, by the factor of e^{λ}, in each iteration) [12,16–18,33].

Unfortunately, there are a number of problems with Lyapunov exponents as a test for chaos:

1. It is easy to forget that a positive Lyapunov exponent is not a direct indication of chaos [19]. Rather, it is only an indication of sensitivity, which is a necessary but insufficient condition of chaos [17]. It is possible for a sensitive trajectory to be non-chaotic [14] (for example, the simple function $f(x) = 2x$ causes two real numbers $x, y \in \mathbb{R}$ to rapidly diverge and grow arbitrarily far apart over time $t \in \mathbb{N}$ s.t. $|f^{\circ t}(x) - f^{\circ t}(y)| = 2t|x - y|$, and so, by definition, f is sensitive, although it is certainly not chaotic)
2. Higher Lyapunov exponents do not always correspond with higher degrees of chaoticity or even complexity (i.e. a higher complexity can be obtained from a lower exponent [19]).
3. Lyapunov exponents are limited to distinguishing between regularity and chaos and fail on other types of intermediate dynamics, such as quasiperiodic dynamics and strange non-chaotic attractors (SNAs) [21].

3.2.2. Fractal dimensions

Definitions of chaos have failed to recognise the inherent *fractal* nature of chaotic systems [34]. Fractals are special types of patterns with a nested structure. Put precisely, a fractal is a set that exhibits a degree of *self-similarity* (i.e. it remains quantitatively similar in its spatial characteristics under contraction, magnification and bounded deformation [16]). Not only are chaotic trajectories known to produce fractals [34], but it has been proposed, informally, that chaotic attractors *are* fractals [34].

A *fractal dimension* is the most common numerical measure used to quantify a fractal [16,35]. In contrast to Lyapunov exponents (which characterises the dynamical properties of trajectories on attractors), the fractal dimension focuses on the geometry of an attractor [12].

There are many approaches to calculate the fractal dimension (including but not limited to the topological dimension, Hausdorff dimension, self-similarity dimension, box-counting dimension, capacity dimension, information dimension, Euclidean dimension, correlation dimension, Lyapunov dimension, and more [12,36]). Even the Hurst exponent, a statistical measure of roughness, is very closely related to the fractal dimension [7,37]. Irregardless of the method, a non-integer *fractal dimension* is a typical signature of chaotic attractors [16] and a fractal *dimension curve* can be used to distinguish clearly between chaotic and regular trajectories (each showing very different dimension curves) [36].

However, fractal dimensions are also not a direct measure of chaos. Rather, they measure fractals and, to the best of our knowledge, a formal definition clarifying the exact relationship between fractals and chaos has yet to be established.

4. The 0–1 test for chaos

The *0–1 test for chaos* is a new, very simple, binary test for distinguishing between regular and chaotic dynamics [5,18,20,21]. In contrast to the usual method of computing the maximal Lyapunov exponent, this test is straightforward to implement [20,22] and computationally inexpensive [18,21,22] (working directly on the time-series data without the need for phase-space reconstruction [18,22,38]). Moreover, the test is universally applicable since it is independent of the origin, nature and dimension of the data fed into the dynamical system under consideration (i.e. the form of the system's equations do not need to be known) [18,22].

A qualitative distinction between this test and other tests for chaos is its ability to detect weak chaos [22] and transitions that occur without Lyapunov exponents turning positive [21] such as with strange non-chaotic attractors (SNAs) [20,21] which are neither chaotic nor quasiperiodic and return an intermediate value $0 < K < 1$.

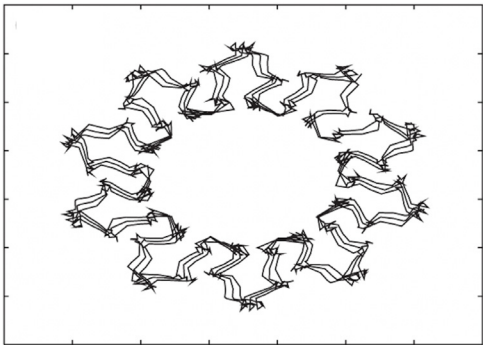

Fig. 4. Power spectrum plots $(\mathrm{Re}(\overline{z}^c) \times \mathrm{Im}(\overline{z}^c))$ of nonchaotic dynamics are typically bounded.

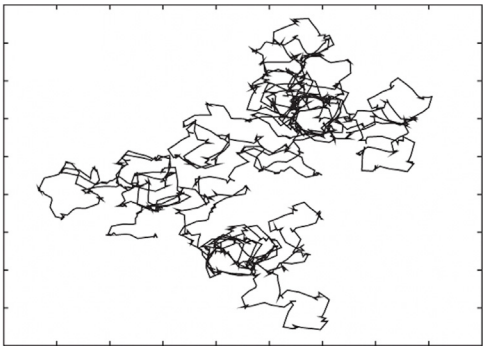

Fig. 5. Power spectrum plots $(\mathrm{Re}(\overline{z}^c) \times \mathrm{Im}(\overline{z}^c))$ of chaotic dynamics tend to grow diffusely.

Definition 16. The 0–1 test for chaos is not applied directly to a trajectory $\mathcal{O}^T(x)$, but rather to a time-series of ***observations*** $\overline{\Phi} \in \mathbb{R}^T : \overline{\Phi} = (\overline{\Phi}_0, \ldots, \overline{\Phi}_{T-1})$, s.t. $\forall t \in [0, T)$:

$$\overline{\Phi}_t = \phi(\ [\mathcal{O}^T(x)]_t\ ) \tag{12}$$

where the exact form of $\phi : \mathbb{S}^W \to \mathbb{R}$ is irrelevant to the test (highlighting its universality).

Definition 17. The time-series of observations $\overline{\Phi}$ is ***transformed into a complex-valued series*** $\overline{z}^c \in \mathbb{C}^T : \overline{z}^c = (\overline{z}^c_0, \ldots, \overline{z}^c_{T-1})$ parameterised by some arbitrary angle $c \in [0, 2\pi]$ s.t. $\forall \tau \in [1, T]$

$$\overline{z}^c_\tau = \sum_{t=0}^{\tau} \overline{\Phi}_t e^{itc} \tag{13}$$

The dynamics are characterised by how the variance of the trajectory scales with time in the power spectrum [5,21,39]. For nonchaotic trajectories with regular motion (i.e. periodic or quasiperiodic dynamics), the growth of the transformed trajectory, $\overline{z}^c$, is typically bounded and exhibits no drift (Fig. 4) [5, 20,22], ensuring the mean square displacement is a bounded function in time [18,39].

Whereas for chaotic trajectories, the transformed trajectory behaves asymptotically and grows diffusely, like a two-dimens ional Brownian motion with zero drift (Fig. 5) [5,20,22], ensuring the mean square displacement scales linearly with time [18,39].

Definition 18. The *smoothed* ***mean square displacement*** vector $\overline{M}^c_n \in \mathbb{R}^N$ is a convenient method for distinguishing whether $\overline{z}^c$ has a bounded or diffusive growth rate. Let $\|.\| = \mathrm{Re}(.)^2 + \mathrm{Im}(.)^2$

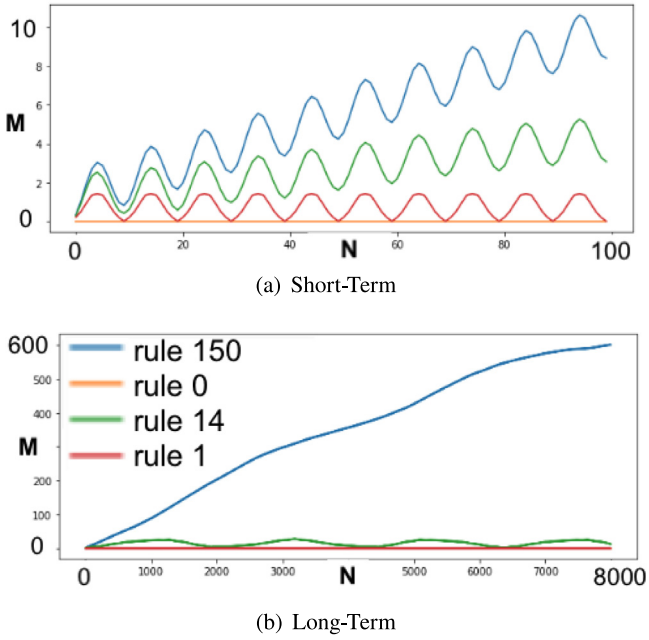

(a) Short-Term

(b) Long-Term

Fig. 6. Examples of the mean square displacement M^c for regular and chaotic dynamics, including: rule 0, ρ_0 (a point attractor), rule 1, ρ_1 (a limit cycle), rule 14, ρ_{14} (a toroidal attractor) and rule 150, ρ_{150} (a strange attractor)

Table 2
Expected outcomes for a chaotic and non-chaotic trajectory, $\mathcal{O}^T(x)$, its growth pattern in the power spectrum, $\overline{z}^c$, mean square displacement, $\overline{M}^c$, and resulting correlation coefficient, K.

$\mathcal{O}^T(x)$	$\overline{z}^c$	$\overline{M}^c$	K
Non-chaotic	bounded	bounded	0
Chaotic	diffusive	linear	1

and $N \in \mathbb{N} : N \ll T$ then $\forall n \in [1, N]$:

$$\overline{M}^c_n = \frac{1}{T-N} \sum_{t=0}^{T-N} \|\overline{z}^c_{t+n} - \overline{z}^c_t\| \tag{14}$$

Definition 19. The ***correlation coefficient*** vector $\overline{K}^c \in \mathbb{R}^N$ represents the log–log plot of mean square displacement $\forall n \in [1, N]$:

$$\overline{K}^c_n = \lim_{n \to \infty} \frac{\log \overline{M}^c_n}{\log n} \tag{15}$$

Definition 20. We obtain the final ***asymptotic growth rate***, $K^c \in [0, 1]$, by applying linear regression to $\overline{K}^c$. After repeating for $I \in \mathbb{N} : I \geq 1$ angles, the median is taken as the ***final classifier***:

$$K = median\{K^c \mid c \in [0, 2\pi]\} \tag{16}$$

In this way, all the information relevant for chaoticity or regularity is condensed into a single scalar value, K, that effectively captures the strength of the linear growth [5,18,21,22]. When the underlying dynamics are regular, the test yields an output close to $K = 0$, with probability one but $K = 1$ for sufficiently chaotic dynamics [18,20,21,38].

5. Experiment

The 0–1 test for chaos is universally applicable to any deterministic dynamical system and has already found a wide range of

applications within areas such as finance and economics [40,41], engineering [42,43], electronics [44], multi-agent systems [45], traffic dynamics [46], fluid dynamics [47], dissipative systems [48,49], Hamiltonian systems [50], discrete systems, partial differential equations, etc. In addition, we aim to utilise the 0–1 test for the automatic classification of ECA dynamics.

5.1. Setup

The 88 equivalent rule classes were tested using an ECA lattice width equal to that used by Wolfram in his classification (Section 5.2.2), $W = 637$, a trajectory depth of $T = 50{,}000$ and a fixed initial configuration (IC), $x \in \mathbb{S}^W$, selected at random from a set of configurations with an approximately equal density of 0s and 1s (see our github repository[2] for the exact IC used).

An ECA trajectory, $\mathcal{O}^T(x)$, is then converted into a sequence of observations (Definition 16) by taking the gray encoding of each configuration and expressing it as a decimal (normalised to be within the range 0 and 1):

$$\phi(x) = \frac{1}{2^W} \sum_{w=1}^{W} 2^{W-w}(x_w \oplus x_{w+1}) \tag{17}$$

Our Python implementation of the 0–1 Test for chaos (algorithm 1) was run using the following parameters: $N = \frac{T}{3} = \frac{50{,}000}{3} \approx 16{,}666$ and $I = 5$ angles (whereby the ith angle is calculated as $c = \frac{i\pi}{20}$). The result, K, of each rule, ρ, was recorded[3] and grouped by common patterns exhibited in the power spectrum (Section 5.2.1) in Table 3.

Algorithm 1: The 0–1 Test for Chaos

$\overline{\Phi} \leftarrow (\phi(\hat{x}) \mid \hat{x} \in \mathcal{O}^T(x))$; // Def16
$N \leftarrow \frac{T}{3}$
$I \leftarrow 5$
for $i \in [1, I]$ **do**
  $c \leftarrow \frac{i\pi}{20}$; // i-th angle
  for $\tau \in [1, T]$ **do**
    $\overline{z}^c_\tau \leftarrow \sum_{t=0}^{\tau} \overline{\Phi}_t e^{itc}$; // Def17
  end
  $\overline{z}^c \leftarrow (\overline{z}^c_1, \ldots, \overline{z}^c_T)$
  for $n \in [1, N]$ **do**
    $\overline{M}^c_n \leftarrow \frac{1}{T-N} \sum_{t=0}^{T-N} ||\overline{z}^c_{t+n} - \overline{z}^c_t||$; // Def18
    $\overline{K}^c_n \leftarrow \frac{\log \overline{M}^c_n}{\log n}$; // Def19
  end
  $K_i \leftarrow linear\_regression\{\overline{K}^c_1, \ldots, \overline{K}^c_N\}$;
end
$K \leftarrow median\{K_1, \ldots, K_I\}$; // Def20

5.2. Analysis of results

5.2.1. Types of spectral patterns

The test is easily automated and, while it is not necessary to make a visual interpretation of the results, the growth patterns may be visualised by plotting the real and imaginary components of $\overline{z}^c$. Upon a qualitative inspection of each rule's growth in the power spectrum, chaotic rules were confirmed to exhibit the expected brownian motion. Unexpectedly, three distinct types of bounded spectral patterns were discovered for nonchaotic dynamics (Fig. 8).

[2] https://github.com/mohammedterryjack/0-1Test/blob/main/run_experiment.ipynb

[3] https://raw.githubusercontent.com/mohammedterryjack/0-1Test/main/experiments/results/t=50000.csv

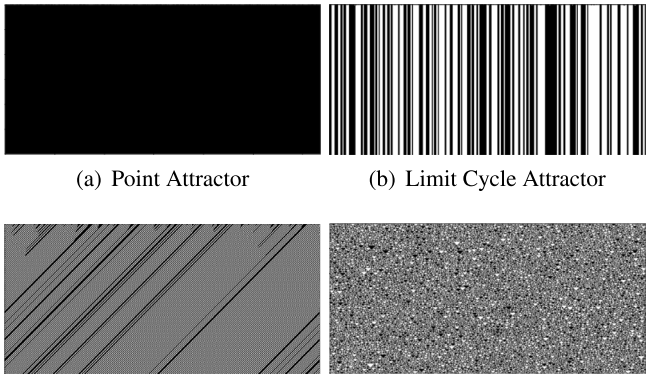

(a) Point Attractor (b) Limit Cycle Attractor

(c) Toroidal Attractor (d) Strange Attractor

Fig. 7. Example spacetime trajectories, $\mathcal{O}^T(x)$, of three nonchaotic rules (a) ρ_0, (b) ρ_1, (c) ρ_{14} and one chaotic rule (d) ρ_{150}.

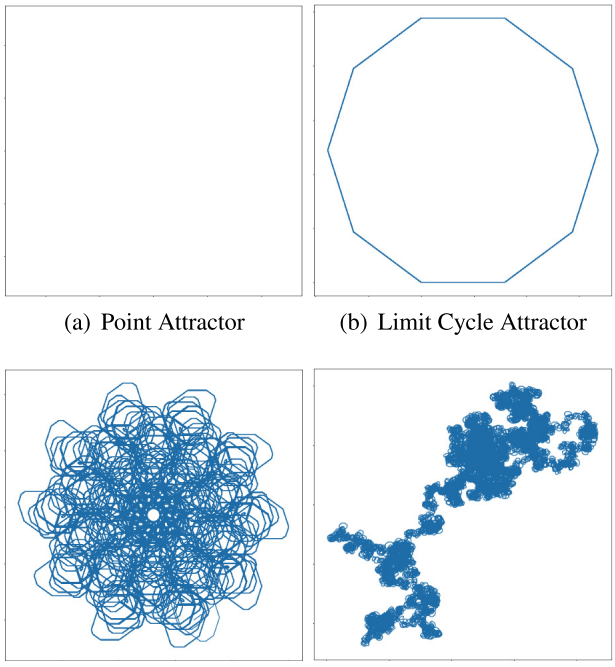

(a) Point Attractor (b) Limit Cycle Attractor

(c) Toroidal Attractor (d) Strange Attractor

Fig. 8. Example of power spectrum plots ($\mathrm{Re}(\overline{z}^c) \times \mathrm{Im}(\overline{z}^c)$) for the transformed trajectories, $\overline{z}^c$, of three nonchaotic rules (a) ρ_0, (b) ρ_1, (c) ρ_{14} and one chaotic rule (d) ρ_{150}.

- We identified 8 nonchaotic rules governed by a *Point Attractor* (an attractor of linear dissipative systems whose trajectories converge to a single steady state, as shown in Fig. 7(a)). These rules share a common power spectrum growth which is bound to a single point (Fig. 8(a)). Therefore, their resulting correlation coefficients are exactly $K = 0.00$.
- ◯ We identified 31 nonchaotic rules governed by a *Limit Cycle Attractor* (an attractor which causes trajectories to form a periodic cycle with regularly repeating behaviour which is easily predictable, as shown in Fig. 7(b)). These rules all exhibit a common power spectrum growth which is bound to a closed loop (Fig. 8(b)). Therefore, their resulting correlation coefficient is also exactly $K = 0.00$.
- ◎ We identified 37 nonchaotic rules governed by a *Toroidal Attractor* (an attractor which looks like a large doughnut or bagel with geometrical characteristics of a torus due to the

Table 3
0–1 Test Results.

	Spectral Pattern	Rules (ρ)	0–1 (K)	Test
•	Point Attractor	0, 8, 32, 40, 128, 136, 160, 168	0.00	Regular
◯	Limit Cycle Attractor	1, 4, 5, 12, 13, 19, 23, 28, 29, 33, 36, 37, 44, 50, 51, 72, 73, 76, 77, 78, 104, 108, 132, 140, 156, 164, 172, 178, 200, 204, 232	0.00	Regular
◎	Toroidal Attractor	62, 94, 184 57 58 27, 35 9, 138 3, 25, 43, 134 10, 14, 15 7, 11, 142, 162 34, 42, 56, 74, 130, 152, 170 2, 24, 46 6, 18, 38 126 41 26 154	0.00 0.01 0.05 0.06 0.07 0.08 0.09 0.10 0.11 0.12 0.13 0.32 0.39 0.53 0.75	Regular
〰	Strange Attractor	110 54 45, 60, 90, 106 22, 30, 105, 122, 146, 150	0.95 0.97 0.99 1.00	Chaotic

superposition of different shifting spirals over many planes, that eventually cycle back on itself exactly or inexactly. Unlike limit cycle attractors, each cycle in a toroidal attractor is not identical to the last due to this shift, causing the cycles to drift over the course of a larger cycle, leaving toroidal attractors with a very large period. Toroidal attractors produce either periodic dynamics, as shown in Fig. 7(c), or quasiperiodic dynamics). These rules display a common type of power spectrum pattern which is bound to the region of a torus (Figs. 8(c), 9, 14(a) and 14(b)). Therefore, their resulting correlation coefficient is close to $K \approx 0$. Rules like ρ_{41} had very large periods ($\tau \approx 250,000$) which resulted in misleadingly high test values, K (however, their values approach $K = 0$ as their trajectory length increases).

〰 We identified 12 chaotic rules governed by a *Strange Attractor* (an attractor which generates highly complex, aperiodic trajectories with chaotic dynamics, as shown in Figs. 7(d) and 21(b)). In the power spectrum, these rules all have unbounded growths which resemble brownian motion (Figs. 5, 8(d) and 22(b)). Their resulting correlation coefficients are between $K = 0.95 - 1.00$.

5.2.2. Quantitative vs qualitative classifications

Stephen Wolfram [6] simulated thousands of ECAs with lattice widths $W = 637$ to a depth of $T = 318$ from a single, identical initial configuration, $x' \in D_{0.5}$, chosen at random from a subset of configurations with 0.5 densities, $D_{0.5} = \{x \in \mathbb{S}^W \mid \sum_{w=1}^{W} x_w = \frac{W}{2}\}$ [4]. By relying on *"how things look to our eyes"* [6], Wolfram proposed there exist four unique classes of behaviour:

W1: **Homogeneous fixed points** [7] (Fig. 10): evolutions toward uniform, quiescent configurations [4,51] with zero temporal and spatial entropy [52,53] and the lowest Kolmogorov complexity (i.e. an asymptotic compressibility ratio of 0).

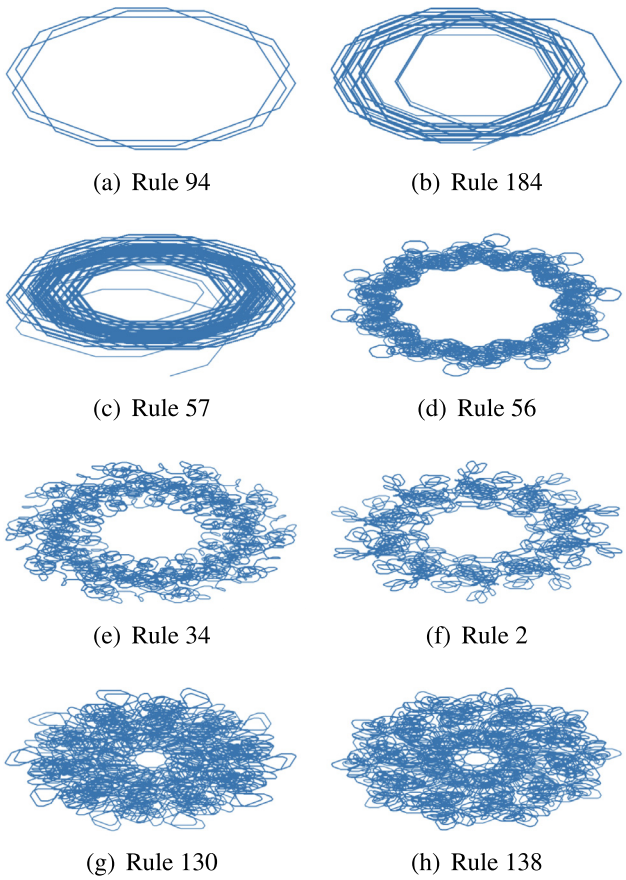

Fig. 9. Example of power spectrum plots ($\mathrm{Re}(\overline{z}^c) \times \mathrm{Im}(\overline{z}^c)$) for the transformed trajectories, $\overline{z}^c$, of several nonchaotic (toroidal attractor) rules (a) ρ_{94}, (b) ρ_{184}, (c) ρ_{57}, (d) ρ_{56}, (e) ρ_{34}, (f) ρ_2, (g) ρ_{130}, (h) ρ_{138}.

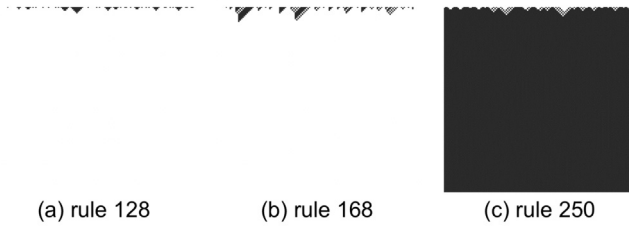

Fig. 10. Wolfram's Class I (W1).

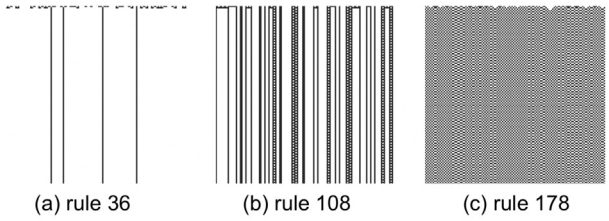

Fig. 11. Wolfram's Class II (W2)

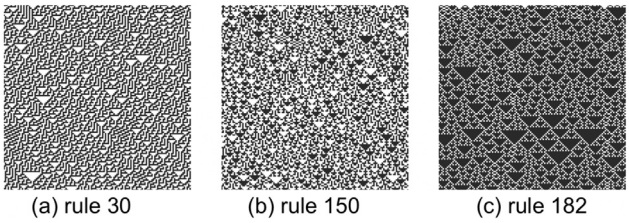

Fig. 12. Wolfram's Class III (W3)

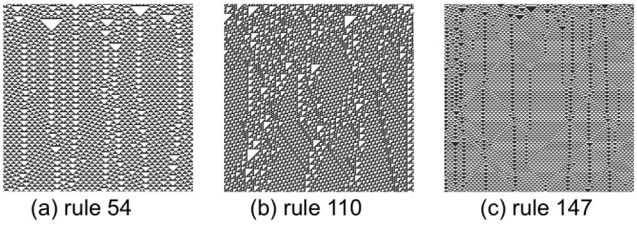

Fig. 13. Wolfram's Class IV (W4)

W2: **Spatially inhomogeneous fixed points** (Fig. 11): evolutions toward temporally periodic configurations [4,51] with zero temporal entropy but positive spatial entropy [52] and low Kolmogorov complexities (i.e. compressibility ratios less than 1/2 [53].

W3: **Strange (chaotic) attractors** (Fig. 12): complex chaotic aperiodic evolutions [4,7] with positive spatial and temporal entropy [52] and the highest Kolmogorov complexity (i.e. almost incompressible) [53].

W4: **Strange (weakly chaotic) attractors** (Fig. 13): complex quasiperiodic evolutions [4,7] with localised structures, sometimes long-lived (comparable to biological systems or self-organising, computational systems [51]) and asymptotic compressibility ratios equal to 1 [53]. Often described as an intermediate, transition phase between classes W2 and W3 (i.e. between order and chaos) and thus informally referred to as *the edge of chaos*

Wolfram's classification renewed public interest in CA research and became very popular. However, many perceived his qualitative and, ultimately, subjective approach to be the classification's greatest drawback [8,54,55]. Wolfram maintained that his heuristic approach was actually a strength of the classification, as opposed to a weakness, because it leverages the unparallelled pattern recognition capabilities of the human mind; *"despite all the various methods of mathematical and other analysis that have been developed, our visual system still represents one of the most powerful and reliable tools we have"* [6].

Unfortunately, without precisely formalised mathematical definitions for each class, there is no effective criteria for membership, nor any quick tests to distinguish classes from one another [2,3,7–10]. Therefore, many successive works in the field have tried to find well-formalised classifications, utilising various ways to quantify interesting characteristics of ECAs. For example, Kurka [56] suggests the following dynamical properties to precisely describe Wolfram's classes:

W1: $\mathcal{O}^T(x)$ is *equicontinuous* (Definition 7)
W2: $\mathcal{O}^T(x)$ is *almost equicontinuous* (Definition 8)
W3: $\mathcal{O}^T(x)$ is *sensitive* (Definition 9)
W4: $\mathcal{O}^T(x)$ is *positively expansive* (Definition 10)

When comparing the famous qualitative classification of Stephen Wolfram (Section 5.2.2) with the quantitative results given by the 0–1 Test for Chaos (Table 4), we notice the following similarities and differences:

W1: Wolfram's class 1 rules (Fig. 10) all test as nonchaotic, $K = 0$, in agreement with the definition of the class given by Wolfram definition (Section 5.2.2). Furthermore, these rules exactly correspond with the nonchaotic rules exhibiting a point attractor in their power spectrum plots.

W2: Wolfram's class 2 rules (Fig. 11) also all test as nonchaotic, $K = 0 - 0.75$, in agreement with their class definition (Section 5.2.2). These rules consist of every rule exhibiting a limit cycle attractor in their power spectrum as well as all but three rules exhibiting toroidal attractors. Wolfram may not have considered the distinction between these two types of dynamics in his classification since their spacetime diagrams appear similar (if the space and time axes are considered equivalently); i.e. dynamics governed by a limit cycle typically appear as vertical lines (Fig. 7(b)) whereas dynamics governed by a toroidal attractor typically appear as diagonal lines (Fig. 7(c)).

W3: The majority of Wolfram's *chaotic* class 3 rules (Fig. 12) are confirmed as chaotic by the 0–1 test, $K = 0.99 - 1.00$. However, there is an exception for a couple rules (i.e. rule 18 and 126) which actually test as nonchaotic, $K = 0.13 - 0.32$, and exhibit toroidal attractor spectral patterns (Fig. 14). After approximately 350 time steps, $\tau \approx 350$, these rules periodically repeat their spacetime patterns, which is a clear confirmation of their regular, nonchaotic nature (nonchaotic dynamics governed by toroidal attractors may be as complex as chaos, but their regular nature make them predictable. Chaos, on the other hand, is both complex and unpredictable [57]). It is understandable how these complex nonchaotic dynamics could be confused for complex chaotic dynamics in Wolfram's qualitative classification, as the complexity of their spacetime pattern make their periodic nature difficult to detect by eye (Figs. 15 and 16).

W4: Wolfram's class 4 rules (Fig. 13) also test as chaotic, $K = 0.95 - 0.99$, but the range of values are slightly lower than those of class 3 rules, $K = 0.99 - 1.00$, which may indicate a weaker form of chaos (inline with the class' description as being 'weakly chaotic'). In the class' description, Wolfram posited that certain features, like emergent particles,

Table 4
Comparing the 0–1 Test Results against Wolfram's Classification.

W. Class	Rules (ρ)	0–1 Test Result	Spectral Pattern	(K)
W1	0, 8, 32, 40, 128, 136, 160, 168	Regular	• Point	0.00 - 0.00
W2	1, 4, 5, 12, 13, 19, 23, 28, 29, 33, 36, 37, 44, 50, 51, 72, 73, 76, 77, 78, 104, 108, 132, 140, 156, 164, 172, 178, 200, 204, 232	Regular	◯ Limit Cycle	0.00 - 0.00
	2, 3, 6, 7, 9, 10, 11, 14, 15, 24, 25, 26, 27, 34, 35, 38, 42, 43, 46, 56, 57, 58, 62, 74, 94, 130, 134, 138, 142, 152, 154, 162, 170, 184		◎ Toroidal	0.00 - 0.75
W3	18, 126	Regular	◎ Toroidal	0.13 - 0.32
	22, 30, 45, 60, 90, 105, 122, 126, 146, 150	Chaotic	⇜⇝ Strange	0.99 - 1.00
W4	41	Regular	◎ Toroidal	0.39 - 0.39
	54, 106, 110	Chaotic	⇜⇝ Strange	0.95 - 0.99

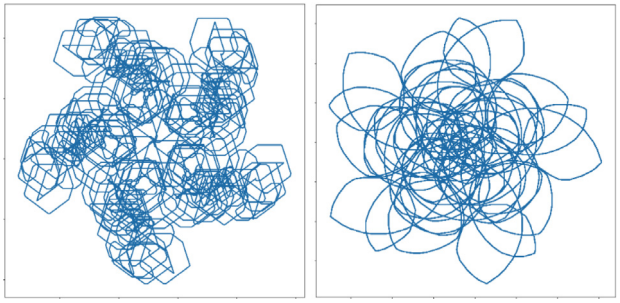

(a) Rule 18 (b) Rule 126

Fig. 14. Example power spectrum plots ($\mathrm{Re}(\overline{z}^c) \times \mathrm{Im}(\overline{z}^c)$) for the transformed trajectories, $\overline{z}^c$, of rules (a) ρ_{18} and (b) ρ_{126}, showing toroidal attractors.

are unique to class 4 rules. However, it is also plausible that such features are common to all chaotic rules and the complexity of strongly chaotic rules obscure the visibility of these features (similar to the way in which the periodicity of rules 18 and 126 become camouflaged). Rule 41 is the only exception to the class 4 rules because it is nonchaotic according to the 0–1 test, $K = 0.39$, exhibiting a toroidal attractor in its power spectrum. Rule 41 happens to have an incredibly long period, $\tau \approx 250,000$, meaning its regularity went unnoticed by Wolfram when viewing its spacetime pattern (if a periodic trajectory has an extremely long period which is greater than the observed trajectory, $\tau \geq T$, it appears indistinguishable from a non-periodic trajectory because it has not been observed long enough to see the orbit closing [12,23]). Even if it were to be viewed long enough to permit a single repetition to occur, $T > 500,000$, it would render the spacetime too zoomed-out to have any discernible details (highlighting another advantage of quantitative approaches over qualitative classifications).

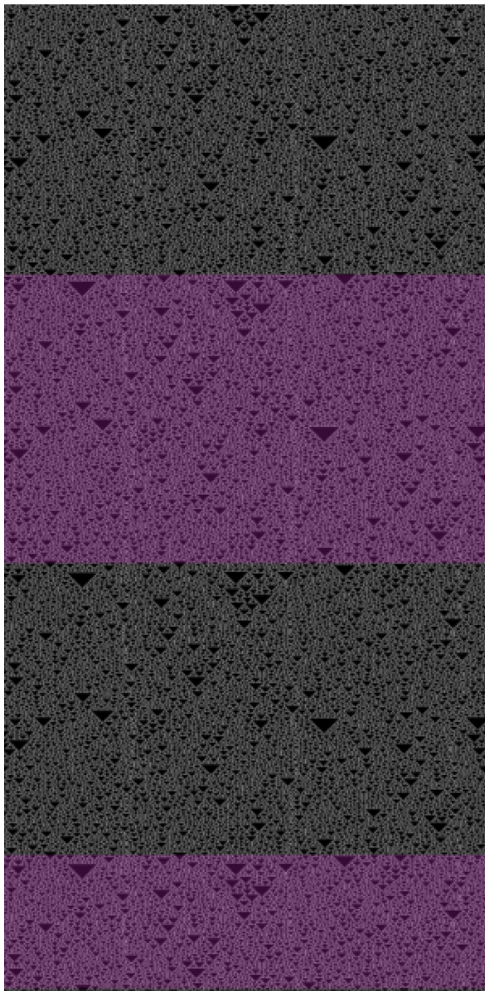

Fig. 15. Example spacetime trajectory $\mathcal{O}^T(x)$ of rule 18 ρ_{18} showing complex non-chaotic dynamics (purple highlights facilitate recognition of the repeating pattern).

5.2.3. Chaoticity vs complexity

Linear separability (Section 2.2.3) is a vital concept in Chua's definition of *complexity*. The *Chua complexity index*, $\kappa \in \mathbb{Z}$, is the minimum number of hyperplanes, h, needed to separate the bipolar vertices of a hypercube [26,58]. In this way, the geometrical structure of a local rule (represented as a hypercube, Section 2.2.2) can be quantified and used as a measure of the rule's intrinsic complexity. There are exactly 14 ways to uniquely colour a 3D hypercube and all ECA rules, ρ, can be mapped to one of these unique colour combinations (hypercube structures), $\varrho : \mathbb{S}^{2r+1} \rightarrow \mathbb{S}$ (Table 5).

Table 5
ECA rules, ρ, mapped to their respective hypercube structures, ϱ, of varying intrinsic complexity, κ.

Hypercube Structure (ϱ)	ECA Rules (ρ)	Chua Complexity (κ)
I (Eq. (18))	0	0
II (Eq. (19))	1, 2, 4, 8, 32, 128	1
III (Eq. (20))	3, 5, 10, 12, 34, 136, 160	
IV (Eq. (21))	7, 11, 13, 14, 19, 35, 42, 50, 76, 138, 140, 162, 168, 200	
V (Eq. (22))	15, 51, 170, 204	
VI (Eq. (23))	23, 43, 77, 142, 178, 232	
VII (Eq. (24))	6, 9, 18, 33, 40, 72, 130, 132	2
VIII (Eq. (25))	24, 36, 126	
IX (Eq. (26))	25, 26, 28, 37, 38, 44, 56, 62, 74, 94, 110, 122, 152, 164	
X (Eq. (27))	30, 45, 54, 57, 106, 108, 154, 156	
XI (Eq. (28))	22, 41, 73, 104, 134, 146	
XII (Eq. (29))	60, 90	
XIII (Eq. (30))	27, 29, 46, 58, 78, 172, 184	3
XIV (Eq. (31))	105, 150	

$\kappa = 0$

The rules associated with ϱ_{I} are the simplest because all vertices in the hypercube are the same colour, and therefore do not require separating, or in other words, require 0 hyperplanes, $\kappa = 0$.

$$\varrho_{\text{I}}(v) = 0 \tag{18}$$

$\kappa = 1$

All rules requiring a single hyperplane, $\kappa = 1$, are linearly separable and known as 'threshold functions' (Section 2.2.3)

$$\varrho_{\text{II}}(v) = v_1 v_2 v_3 \tag{19}$$

produces true points $V_\top = \{(1, 1, 1)\}$ and false points $V_\bot = \{(0, 0, 0), (0, 0, 1), (0, 1, 0), (0, 1, 1), (1, 0, 0), (1, 0, 1), (1, 1, 0)\}$ which are linearly separable (Fig. 17).

Proof. Let $h = \begin{pmatrix}1.0\\1.0\\1.0\end{pmatrix}$. By Definition 12, ϱ_{II} is a threshold function if $min\{h \cdot v_\top \mid v_\top \in V_\top\} > max\{h \cdot v_\bot \mid v_\bot \in V_\bot\} \Rightarrow min\{3\} > max\{0, 1, 1, 2, 1, 2, 2\} \Rightarrow 3 > 2$

$$\varrho_{\text{III}}(v) = v_1 v_2 \tag{20}$$

produces true points $V_\top = \{(1, 1, 0), (1, 1, 1)\}$ and false points $V_\bot = \{(0, 0, 0), (0, 0, 1), (0, 1, 0), (0, 1, 1), (1, 0, 0), (1, 0, 1)\}$ which are linearly separable (Fig. 17(b)).

Proof. Let $h = \begin{pmatrix}1.0\\1.0\\0.0\end{pmatrix}$. By Definition 12, ϱ_{III} is a threshold function if $min\{h \cdot v_\top \mid v_\top \in V_\top\} > max\{h \cdot v_\bot \mid v_\bot \in V_\bot\} \Rightarrow min\{2, 2\} > max\{0, 0, 1, 1, 1, 1\} \Rightarrow 2 > 1$

$$\varrho_{\text{IV}}(v) = v_1\ max\{v_2, v_3\} \tag{21}$$

produces true points $V_\top = \{(1, 0, 1), (1, 1, 0), (1, 1, 1)\}$ and false points $V_\bot = \{(0, 0, 0), (0, 0, 1), (0, 1, 0), (0, 1, 1), (1, 0, 0)\}$ which are linearly separable (Fig. 17(c)).

Proof. Let $h = \begin{pmatrix}1.0\\0.5\\0.5\end{pmatrix}$. By Definition 12, ϱ_{IV} is a threshold function if $min\{h \cdot v_\top \mid v_\top \in V_\top\} > max\{h \cdot v_\bot \mid v_\bot \in V_\bot\} \Rightarrow min\{1.5, 1.5, 2\} > max\{0, 0.5, 0.5, 1, 1\} \Rightarrow 1.5 > 1$

$$\varrho_{\text{V}}(v) = v_1 \tag{22}$$

produces true points $V_\top = \{(1, 0, 0), (1, 0, 1), (1, 1, 0), (1, 1, 1)\}$ and false points $V_\bot = \{(0, 0, 0), (0, 0, 1), (0, 1, 0), (0, 1, 1)\}$ which are linearly separable (Fig. 17(d)).

Proof. Let $h = \begin{pmatrix}1.0\\0.0\\0.0\end{pmatrix}$. By Definition 12, ϱ_{V} is a threshold function if $min\{h \cdot v_\top \mid v_\top \in V_\top\} > max\{h \cdot v_\bot \mid v_\bot \in V_\bot\} \Rightarrow min\{1, 1, 1, 1\} > max\{0, 0, 0, 0\} \Rightarrow 1 > 0$

$$\varrho_{\text{VI}}(v) = max\{v_1 v_2,\ v_1 v_3,\ v_2 v_3\} \tag{23}$$

produces true points $V_\top = \{(0, 1, 1), (1, 0, 1), (1, 1, 0), (1, 1, 1)\}$ and false points $V_\bot = \{(0, 0, 0), (0, 0, 1), (0, 1, 0), (1, 0, 0)\}$ which are linearly separable (Fig. 17(e))(see Fig. 18).

Proof. Let $h = \begin{pmatrix}1.0\\1.0\\1.0\end{pmatrix}$. By Definition 12, ϱ_{VI} is a threshold function if $min\{h \cdot v_\top \mid v_\top \in V_\top\} > max\{h \cdot v_\bot \mid v_\bot \in V_\bot\} \Rightarrow min\{2, 2, 2, 3\} > max\{0, 1, 1, 1\} \Rightarrow 2 > 1$

$\kappa = 2$

Chua observed that all linearly separable rules, $\kappa = 1$, fell within Wolfram's classes W1 and W2 (Section 5.2.2) [58] and, thus, never tend toward chaotic or complex evolutions (i.e. Wolfram's classes W3 and W4) [26]. Therefore, Chua concluded that only linearly inseparable rules, $\kappa > 1$, are sufficiently complex for such global behaviours to emerge.

$$\varrho_{\text{VII}}(v) = v_1(v_2 = v_3) \tag{24}$$

$$\varrho_{\text{VIII}}(v) = (v_1 = v_2 = v_3) \tag{25}$$

$$\varrho_{\text{IX}}(v) = max\{(1 - v_1)(1 - v_2),\ v_1 v_2 v_3\} \tag{26}$$

$$\varrho_{\text{X}}(v) = v_1 \oplus (v_2 v_3) \tag{27}$$

$$\varrho_{\text{XI}}(v) = max\{v_1 v_2 v_3, v_1(1 - v_2)(1 - v_3), (1 - v_1)(1 - v_2)v_3\} \tag{28}$$

$$\varrho_{\text{XII}}(v) = v_1 \oplus v_2 \tag{29}$$

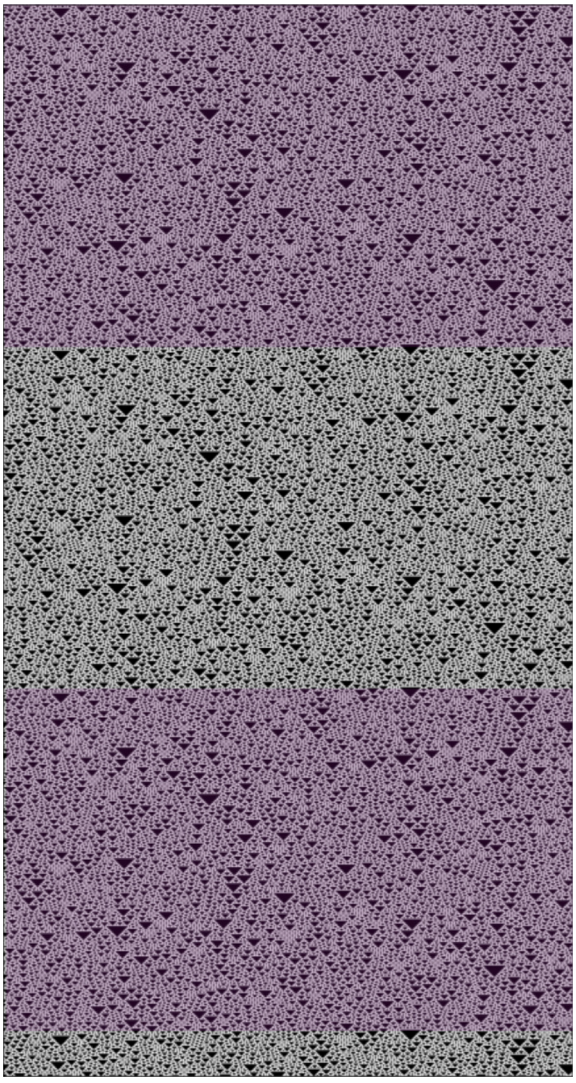

Fig. 16. Example spacetime trajectory $\mathcal{O}^T(x)$ of rule 126 ρ_{126} showing complex non-chaotic dynamics. The regular nature is not easily discernible, due to the high complexity, so purple highlights facilitate recognition of the repeating pattern ($\tau \approx 350$).

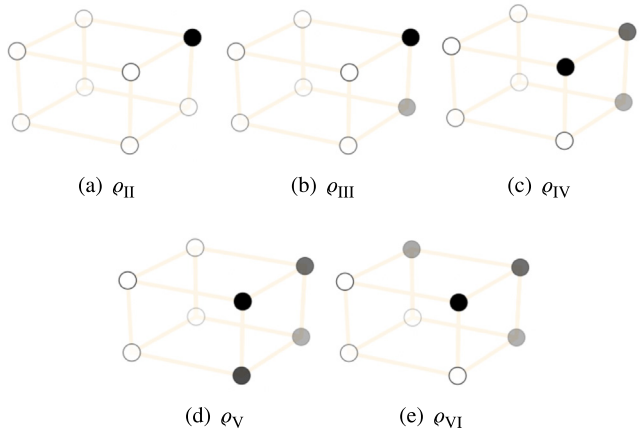

Fig. 17. Hypercube structures, ϱ, which are linearly separable, $\kappa = 1$.

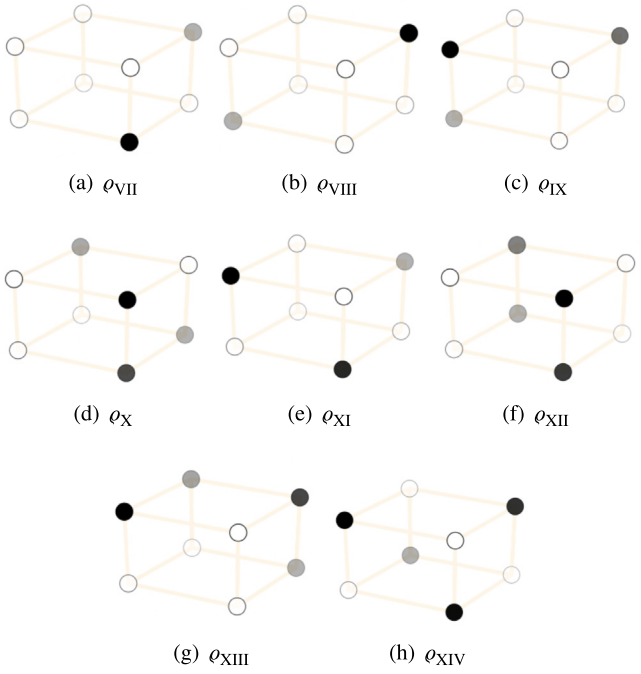

Fig. 18. Hypercubes structures, ϱ, which are linearly inseparable, $\kappa > 1$.

$\kappa = 3$

$$\varrho_{\text{XIII}}(v) = \begin{cases} v_2 & \text{if } v_1 = 1 \\ v_3 & \text{otherwise} \end{cases} \tag{30}$$

$$\varrho_{\text{XIV}}(v) = v_1 \oplus v_2 \oplus v_3 \tag{31}$$

The following relationships were noted when each rule's chaoticity, K, was compared against its complexity, κ (Table 6).

Simple The only rule with a complexity of 0, $\kappa = 0$, was regular, exhibiting a simple point attractor in the power spectrum. Of the 37 linearly separable rules with a complexity of 1, $\kappa = 1$, all were regular, exhibiting either point, limit cycle or toroidal attractors in the power spectrum.

Complex Of the 41 linearly inseparable rules with a complexity of 2, $\kappa = 2$, 31 were regular and 10 were chaotic. Of the 9 linearly inseparable rules with a complexity of 3, $\kappa = 3$, 7 were regular and 2 were chaotic.

Chaotic Chaotic dynamics, $K \approx 1$, seem to only occur above a certain level of complexity (i.e. chaotic rules are only found in rules with a complexity greater than 1, $\kappa > 1$), in accordance with Chua's observation that threshold functions are insufficiently complex for chaotic dynamics to emerge (Section 5.2.3).

Regular However, we find nonchaotic dynamics, $K \approx 0$, occurring in rules of any complexity, $\kappa = 0-3$, which means nonchaotic dynamics are not only found in simple rules, $\kappa \leq 1$, but in highly complex rules too, $\kappa > 1$. This points to an important and counter-intuitive distinction between chaoticity and complexity; chaos is necessarily highly complex but not all highly complex dynamics are necessarily chaotic (since many nonchaotic dynamics can also have highly complex dynamics). For example, rules governed by toroidal attractors have regular, perfectly periodic orbits, which may still produce spacetime patterns as complex as chaos (Figs. 15 and 16).

Table 6
Comparing each rule's 0–1 Test Result (K) against its Chua Complexity Index (κ)

(κ)	Rules (ρ)	0–1 Test Result	Spectral Pattern	(K)
0	0	Regular	• Point	0.00
1	8, 32, 128, 136, 160, 168	Regular	• Point	0.00
	1, 4, 5, 12, 13, 19, 23, 50, 51, 76, 77, 140, 178, 200, 204, 232		◯ Limit Cycle	0.00
	2, 3, 7, 11, 10, 14, 15, 34, 35, 42, 43, 138, 142, 162, 170		◎ Toroidal	0.06 - 0.12
2	40	Regular	• Point	0.00
	28, 33, 36, 37, 44, 72, 73, 104, 108, 132, 156, 164		◯ Limit Cycle	0.00
	6, 9, 18, 24, 25, 26, 38, 41, 56, 57, 62, 74, 94, 126, 130, 134, 152, 154		◎ Toroidal	0.00 - 0.75
	22, 30, 45, 54, 60, 90, 106, 110, 122, 146	Chaotic	⟿ Strange	0.95 - 1.00
3	29, 78, 172	Regular	◯ Limit Cycle	0.00
	27, 46, 58, 184		◎ Toroidal	0.00 - 0.06
	105, 150	Chaotic	⟿ Strange	1.00 - 1.00

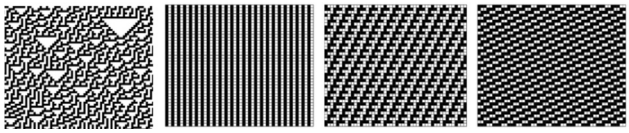

Fig. 19. Rule 30, ρ_{30}, showing chaotic and periodic dynamics depending on its initial configuration.

As such, it is important not to confuse the 0–1 test as a complexity metric because regular rules will always result in near-zero test scores, $K \approx 0$, to indicate their low chaoticity (irregardless of their potentially high complexity).

6. Discussions

6.1. Rules vs initial configurations

It is still unclear exactly which properties of the local rule, ρ, influence the global behaviour [32] (making the connection between the global behaviour of a CA and its local rule explicit is one of the most interesting and challenging problems in CA theory [32]). What has become evident, however, is that the typical long-term behaviour of a CA depends on more than just the local rule, ρ.

While it is fairly obvious that the lattice size can impact the resulting dynamics (since smaller lattices may be unable to unfold the full dynamical potential of the rule [59]), many examples have also been found demonstrating the IC's influence on the resulting dynamics [60] (e.g. rule 40, ρ_{40}, is ordered when starting from a configuration of all 0s but chaotic when starting from random ICs [54]. Rule 106, ρ_{106}, generates simple dynamics from an IC of all 0s bar a single 1, $(\ldots, 0, 0, 1, 0, 0, \ldots)$, yet becomes dynamically complex from an IC of all 0s containing two adjacent 1s $(\ldots, 0, 0, 1, 1, 0, 0, \ldots)$ [60]. The infamously chaotic rule 30, ρ_{30}, can suddenly exhibit periodic behaviour for some ICs [6], as shown in Fig. 19).

Since rules have been shown to belong to different classes of dynamics depending on the exact IC, x, it is slightly misleading to provide a single classification result for each rule, ρ. Nevertheless, due to the impracticality of taking the rule's average dynamics over all possible ICs, it is fairly common for researchers to use a single IC chosen at random (as was specified in our experimental setup in Section 5.1), with the assumption that the rule's typical dynamical behaviour (i.e. the dynamics most often expressed by the rule across all its ICs) will be captured by doing so.

6.2. Pros & cons of the 0–1 test

The 0–1 test for chaos is a proper mathematical test which successfully distinguishes between regular and chaotic dynamics in deterministic systems (such as ECAs) based on a complex-valued transformation of the input time series $\overline{z}^c$ (Definition 17) and a theorem which states that non-chaotic behaviour in this domain is bounded whereas chaos is not, but rather behaves diffusely of the mean zero random walk (Definition 17). The property of the power spectrum is quantified using the mean-square displacement (Definition 18) and extracted into a single number K which represents the median asymptotic growth rate (Definitions 19 and 20). If the underlying dynamics are regular (i.e. periodic, quasiperiodic, etc.) then $K \approx 0$ and if they are chaotic then $K \approx 1$ (Table 2).

Unlike more traditional tests for chaos which rely on phase-space reconstructions, the 0–1 test bypasses the explicit computation of the power spectrum making it very easy to compute, straightforward to implement [20,22] and computationally inexpensive [18,21,22]. Moreover, the test is universally applicable since it is independent of the origin, nature and dimension of the data fed into the dynamical system under consideration [18,22]. This made the 0–1 test a convenient and computationally efficient tool for diagnosing ECA dynamics.

The test does have some known disadvantages. For instance, it requires a carefully chosen angle c in Definition 17 to avoid the occurrence of resonance triggered for some isolated values of c. In fact, this is why the test is designed to be run over a range of angles c before taking the median result (Definition 20, Fig. 20), to ensure the final K is more robust against outliers caused by resonance.

The number of data points used also has an impact on the results of the test. Fewer data points (i.e. a shorter time-series) runs a greater risk of false results. For instance, the mean-squared displacement of only 100 data points of rule 150 appears to grow and not be bounded, thus indicating chaotic dynamics (Fig. 6(a)). However, this conclusion is premature and the mean-squared displacement of 8,000 data points reveals a bounded growth (Fig. 6(b)), correctly indicating non-chaotic dynamics. We noted some regular rules in our own results with scores higher than

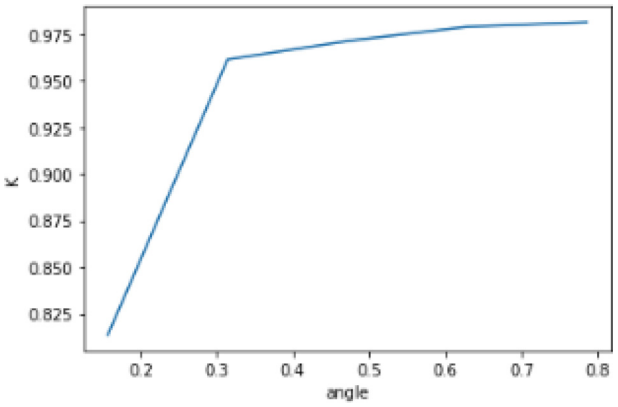

Fig. 20. Correlation coefficients, $\overline{K}^c$, over a range of angles, c, for rule 54, ρ_{54}. The median gives the final 0–1 Test Result, K.

expected (e.g. rule 41 tests highly $K = 0.75$, although it is non-chaotic), despite using 50,000 data points (Section 5.1). However, with probability one K converges to 0 or 1 as $N \to \infty$ and so with more data points the test is guaranteed to provide accurate results.

Interestingly, the binary test was also able to detect a slight difference in the strength of chaos (Section 5.2.2) between Wolfram's chaotic class 3 rules (W3) and the weaker chaotic edge rules (W4). However, we failed to identify a single threshold value for K that would perfectly separate these two classes from one another, which would suggest that the qualitative differences seen between chaos (W3) and the edge of chaos (W4) is not something which is fully captured by the 0–1 test in its current form (or that the proposed class separation is superficially exaggerated and the chaotic edge has far more in common with chaos than not).

6.3. Chaos vs randomness

Given the long-term unpredictability of chaos, it is understandable how it could be confused for *randomness* (e.g. noise), which is also unpredictable. However, randomness is a stochastic process governed nondeterministically, by chance [16], and the probability of appearance of any value in a random sequence is not affected by the knowledge of past values (i.e. values are *mutually independent* [28]). Randomness also lacks any structure, regularities or order [6,12] whereas chaos has readily recognisable structures (i.e. fractals) and regular, nested patterns [6, 34].

Even though randomness (Fig. 21(a)) is stochastic and, unlike deterministic chaos (Fig. 21(b)), is not governed by any attractor, randomness exhibits a diffusive growth pattern in the power spectrum almost identical to that of chaos (Fig. 22) with a mean square displacement that scales linearly (Fig. 23) and a resulting correlation coefficient close to 1, $K \approx 1$ (incorrectly indicating chaos). Misidentifying randomness for chaos is a known weakness of the 0–1 test since it was designed for deterministic dynamical systems [20] as opposed to stochastic systems [18]. While it has been shown to accurately detect regular behaviour within noisy data [22], there is a risk for the test to interpret random data or noise as chaos if it were incorrectly assumed that the data came from a deterministic system [39].

7. Conclusion

The 0–1 Test was used to automatically classify ECA rules (Table 3). Unlike more traditional tests for chaos which rely on

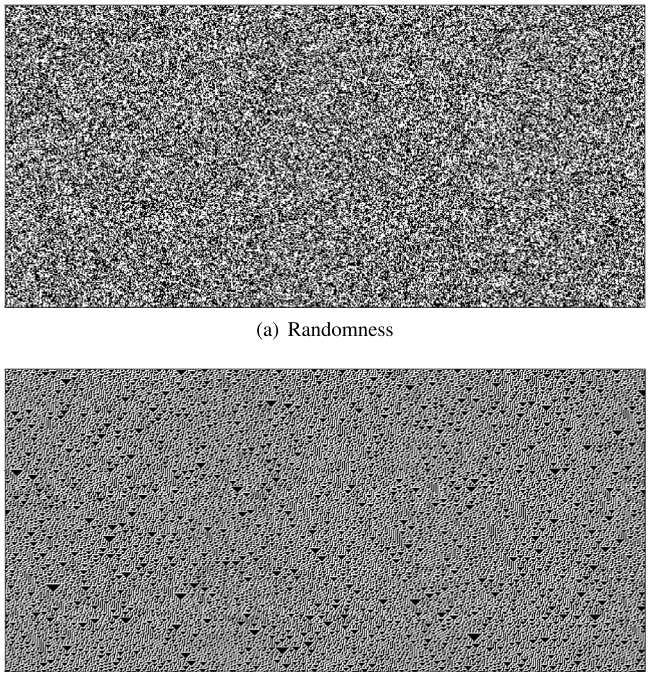

(a) Randomness

(b) Chaos

Fig. 21. Example trajectories $\mathcal{O}^T(x)$ (Definition 5) for (a) stochastic randomness and (b) deterministic chaos, ρ_{30}.

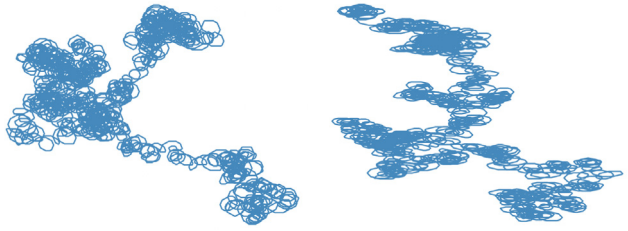

(a) Randomness (b) Chaos

Fig. 22. Example of power spectrum plots $(\mathrm{Re}(\overline{z}^c) \times \mathrm{Im}(\overline{z}^c))$ for the transformed trajectories, $\overline{z}^c$, of (a) a random and (b) chaotic rule, ρ_{30}.

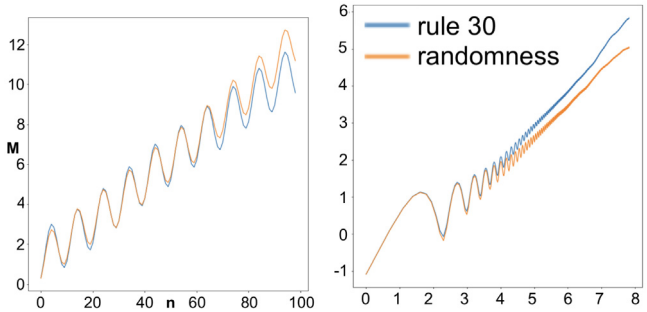

(a) Mean Square Displacement (b) Log-Log plot

Fig. 23. Examples of the mean square displacement M^c for randomness and chaos, ρ_{30}.

phase-space reconstructions, the 0–1 test bypasses the explicit computation of the power spectrum making it very easy to compute, straightforward to implement [20,22] and computationally inexpensive [18,21,22]. Moreover, the test is universally applicable since it is independent of the origin, nature and dimension of the data fed into the dynamical system under consideration [18,

22]. This made the 0–1 test a convenient and computationally efficient tool for diagnosing ECA dynamics.

Upon inspecting each rule's growth in the power spectrum, chaotic rules were confirmed to exhibit the expected brownian motion (Figs. 5, 8(d) and 22(b)). On the other hand, the bounded growths of nonchaotic dynamics unexpectedly revealed three distinct types of spectral patterns (Section 5.2.1). The quantitative results of the 0–1 test were then compared against Wolfram's famous, qualitative classification (Table 4). All class 3 rules, which were classified as chaotic by Wolfram, were also confirmed as chaotic by the 0–1 test, except for two (rule 18 and 126) which are actually periodic (with periods of $\tau \approx 350$) but, due to the high complexity of their spacetime patterns, their periodic nature went undetected by Wolfram (Figs. 15 and 16).

Interestingly, the binary test was also able to detect a slight difference in the strength of chaos (Section 5.2.2) between Wolfram's chaotic class 3 rules (W3) and the weaker chaotic edge rules (W4). The 0–1 test also identified a nonchaotic rule in the 'weakly chaotic' class 4 rules (rule 41), but due to its extremely long period, $\tau \approx 250,000$, which is greater than the observed trajectory, $\tau \geq T$, it was indistinguishable from a non-periodic trajectory because it had not been observed long enough to see its orbit closing [12,23]. Unfortunately, even viewing its spacetime for a timespan long enough to see its repetitive nature would be impractical, as it would render the spacetime too zoomed-out to be discernible in any detail. This highlights yet another advantage of quantitative approaches over qualitative classifications.

Each rule's chaoticity (as quantified by the 0–1 test), was also compared against its complexity (as quantified by its Chua Complexity Index), (Table 6) and it was apparent that a higher level of complexity was necessary for chaotic dynamics to emerge. However, not all highly complex dynamics were necessarily chaotic since nonchaotic dynamics were found in both simple and complex rules (some even as complex as chaos, despite their regular nature, which ultimately meant they were predictable, in direct contrast to chaotic dynamics which are complex and unpredictable [57]). As such, the 0–1 test should not be confused for a complexity metric [11] because, irregardless of a potentially high complexity, nonchaotic dynamics will always result in near-zero scores to indicate their low chaoticity.

A final discussion briefly touches on a problematic assumption underlying the ECA classification task; the local rules are classified irrespective of the IC used, implicitly neglecting any influence the IC may have on the resulting global dynamics (even though rules have been shown to belong to entirely different classes of dynamics depending on the exact IC used). Furthermore, a known limitation of the 0–1 test was discussed; its inability to distinguish between chaos and randomness.

CRediT authorship contribution statement

Mohammed Terry-Jack: Conceptualization, Methodology, Software, Formal analysis, Writing – original draft & editing. **Simon O'Keefe:** Writing – review.

Declaration of competing interest

The authors declare that they have no known competing financial interests or personal relationships that could have appeared to influence the work reported in this paper.

Data availability

No data was used for the research described in the article.

References

[1] B. Aulbach, B. Kieninger, On three definitions of chaos, Nonlinear Dyn. Syst. Theory 1 (1) (2001) 23–37.
[2] G. Cattaneo, M. Finelli, L. Margara, Investigating topological chaos by elementary cellular automata dynamics, Theoret. Comput. Sci. 244 (1–2) (2000) 219–241.
[3] F. Blanchard, J. Cervelle, E. Formenti, Some results about the chaotic behavior of cellular automata, Theoret. Comput. Sci. 349 (3) (2005) 318–336.
[4] G.J. Martinez, A note on elementary cellular automata classification, 2013, arXiv preprint arXiv:1306.5577.
[5] G.A. Gottwald, I. Melbourne, On the implementation of the 0–1 test for chaos, SIAM J. Appl. Dyn. Syst. 8 (1) (2009) 129–145.
[6] S. Wolfram, M. Gad-el Hak, A new kind of science, Appl. Mech. Rev. 56 (2) (2003) B18–B19.
[7] J. De Sales, M. Martins, J. Moreira, One-dimensional cellular automata characterization by the roughness exponent, Physica A 245 (3–4) (1997) 461–471.
[8] G. Cattaneo, C.Q. Vogliotti, The "magic" rule spaces of neural-like elementary cellular automata, Theoret. Comput. Sci. 178 (1–2) (1997) 77–102.
[9] C. Dürr, I. Rapaport, G. Theyssier, Cellular automata and communication complexity, Theoret. Comput. Sci. 322 (2) (2004) 355–368.
[10] J.-C. Dubacq, B. Durand, E. Formenti, Kolmogorov complexity and cellular automata classification, Theoret. Comput. Sci. 259 (1–2) (2001) 271–285.
[11] M. Terry-Jack, Novel lossless compression method based on the Fourier transform to approximate the Kolmogorov complexity of elementary cellular automata, J. Soft. Eng. Appl. 15 (10) (2022) 359–383.
[12] H.-O. Peitgen, H. Jürgens, D. Saupe, M.J. Feigenbaum, Chaos And Fractals: New Frontiers of Science, Vol. 7, Springer, 1992.
[13] J. Banks, J. Brooks, G. Cairns, G. Davis, P. Stacey, On devaney's definition of chaos, Amer. Math. Monthly 99 (4) (1992) 332–334.
[14] C. Mayo-Wilson, Structural chaos, Philos. Sci. 82 (5) (2015) 1236–1247.
[15] G. Cattaneo, E. Formenti, G. Manzini, L. Margara, Ergodicity, transitivity, and regularity for linear cellular automata over zm, Theoret. Comput. Sci. 233 (1–2) (2000) 147–164.
[16] S. Chatterjee, M.R. Yilmaz, Chaos fractals stat., Statist. Sci. 7 (1) (1992) 49–68.
[17] A. Oxley, Detecting the phenomenon of strange non-chaotic attractors, ANZIAM J. 51 (2009) C612–C624.
[18] G.A. Gottwald, I. Melbourne, A new test for chaos in deterministic systems, Proc. R. Soc. Lond. Ser. A Math. Phys. Eng. Sci. 460 (2042) (2004) 603–611.
[19] R. Brown, L.O. Chua, Clarifying chaos II: Bernoulli chaos, zero Lyapunov exponents and strange attractors, Int. J. Bifurcation Chaos 8 (01) (1998) 1–32.
[20] M.-F. Danca, N. Kuznetsov, Hidden strange nonchaotic attractors, Mathematics 9 (6) (2021) 652.
[21] J. Dawes, M. Freeland, The '0–1 test for chaos' and strange nonchaotic attractors, 2008, p. 1210, Preprint 1209.
[22] G.A. Gottwald, I. Melbourne, The 0-1 test for chaos: A review, Chaos Detect. Predict. (2016) 221–247.
[23] H. Thunberg, Periodicity versus chaos in one-dimensional dynamics, SIAM Rev. 43 (1) (2001) 3–30.
[24] L.A. Smith, Predictability and chaos, Encycl. Atmospheric Sci. 4 (2003) 1777–1785.
[25] M. Schüle, R. Stoop, A full computation-relevant topological dynamics classification of elementary cellular automata, Chaos 22 (4) (2012) 043143.
[26] L.O. Chua, S. Yoon, R. Dogaru, A nonlinear dynamics perspective of Wolfram's new kind of science part I: Threshold of complexity, Int. J. Bifurcation Chaos 12 (12) (2002) 2655–2766.
[27] Y. Crama, P.L. Hammer, Boolean Functions: Theory, Algorithms, and Applications, Cambridge University Press, 2011.
[28] C.E. Lobry, Chaos and Cellular Automata.
[29] P. Touhey, Chaos: the evolution of a definition, Irish Math. Soc. Bull (40) (1998) 60–70.
[30] M. Vellekoop, R. Berglund, On intervals, transitivity=chaos, Amer. Math. Monthly 101 (4) (1994) 353–355.
[31] C. Knudsen, Chaos without nonperiodicity, Amer. Math. Monthly 101 (6) (1994) 563–565.
[32] G. Manzini, L. Margara, A complete and efficiently computable topological classification of D-dimensional linear cellular automata over Zm, Theoret. Comput. Sci. 221 (1–2) (1999) 157–177.
[33] C.H. Skokos, G.A. Gottwald, J. Laskar, Chaos Detection and Predictability, Vol. 1, Springer, 2016.
[34] J.P. Crutchfield, J.D. Farmer, N.H. Packard, R.S. Shaw, 1995. Chaos.
[35] G. Boxdorfer, A Study of Visualization Approaches and Fractal Dimension Classification of Certain Boolean Networks (Ph.D. thesis), University of Nebraska at Omaha, 2021.

[36] F. Freistetter, Fractal dimensions as chaos indicators, Celestial Mech. Dynam. Astronom. 78 (1) (2000) 211–225.
[37] Z. Liang, Z. Feng, X. Guangxiang, Comparison of fractal dimension calculation methods for channel bed profiles, Procedia Eng. 28 (2012) 252–257.
[38] G.A. Gottwald, I. Melbourne, On the validity of the 0–1 test for chaos, Nonlinearity 22 (6) (2009) 1367.
[39] J. Hu, W.-w. Tung, J. Gao, Y. Cao, Reliability of the 0-1 test for chaos, Phys. Rev. E 72 (5) (2005) 056207.
[40] K. Webel, Chaos in german stock returns—New evidence from the 0–1 test, Econom. Lett. 115 (3) (2012) 487–489.
[41] B. Xin, J. Zhang, Finite-time stabilizing a fractional-order chaotic financial system with market confidence, Nonlinear Dynam. 79 (2015) 1399–1409.
[42] G. Litak, A. Syta, M. Wiercigroch, Identification of chaos in a cutting process by the 0–1 test, Chaos Solitons Fractals 40 (5) (2009) 2095–2101.
[43] V. Nair, R. Sujith, A reduced-order model for the onset of combustion instability: physical mechanisms for intermittency and precursors, Proc. Combust. Inst. 35 (3) (2015) 3193–3200.
[44] P. Swathy, K. Thamilmaran, Dynamics of SC-CNN based variant of MLC circuit: An experimental study, Int. J. Bifurcation Chaos 24 (02) (2014) 1430008.
[45] F. Leon, Design and evaluation of a multiagent interaction protocol generating behaviours with different levels of complexity, Neurocomputing 146 (2014) 173–186.
[46] B. Krese, E. Govekar, Analysis of traffic dynamics on a ring road-based transportation network by means of 0–1 test for chaos and Lyapunov spectrum, Transp. Res. C 36 (2013) 27–34.
[47] N. Martinsen-Burrell, K. Julien, M.R. Petersen, J.B. Weiss, Merger and alignment in a reduced model for three-dimensional quasigeostrophic ellipsoidal vortices, Phys. Fluids 18 (5) (2006) 057101.
[48] H. Erzgräber, S. Wieczorek, B. Krauskopf, Dynamics of two semiconductor lasers coupled by a passive resonator, Phys. Rev. E 81 (5) (2010) 056201.
[49] T.-L. Tsai, J.H. Dawes, Dynamics near a periodically-perturbed robust heteroclinic cycle, Physica D 262 (2013) 14–34.
[50] C. Skokos, C. Antonopoulos, T. Bountis, M. Vrahatis, Detecting order and chaos in Hamiltonian systems by the SALI method, J. Phys. A: Math. Gen. 37 (24) (2004) 6269.
[51] K. Culik II, L.P. Hurd, S. Yu, Computation theoretic aspects of cellular automata, Physica D 45 (1–3) (1990) 357–378.
[52] K. Sutner, Classification of cellular automata, Encycl. Complex. Syst. Sci. 3 (2009) 755–768.
[53] H. Zenil, E. Villarreal-Zapata, Asymptotic behavior and ratios of complexity in cellular automata, Int. J. Bifurcation Chaos 23 (09) (2013) 1350159.
[54] H. Zenil, Compression-based investigation of the dynamical properties of cellular automata and other systems, 2009, arXiv preprint arXiv:0910.4042.
[55] E. Borriello, S. Imari Walker, An information-based classification of elementary cellular automata, Complexity 2017 (2017).
[56] P. Kurka, Topological Dynamics of One-Dimensional Cellular Automata, Encyclopedia of Complexity and System Sciences, Springer-Verlag, Berlin, 2008.
[57] G. Li, Y. Yue, J. Xie, C. Grebogi, Strange nonchaotic attractors in a nonsmooth dynamical system, Commun. Nonlinear Sci. Numer. Simul. 78 (2019) 104858.
[58] M. Al-Emam, V. Kaurov, Cellular automata complexity threshold and classification: A geometric perspective, Complex Syst. 23 (4) (2014) 355–376.
[59] L. Albantakis, G. Tononi, The intrinsic cause-effect power of discrete dynamical systems—from elementary cellular automata to adapting animats, Entropy 17 (8) (2015) 5472–5502.
[60] J. Machicao, L.C. Ribas, L.F. Scabini, O.M. Bruno, Cellular automata rule characterization and classification using texture descriptors, Physica A 497 (2018) 109–117.